

Self-biased broadband magnet-free linear isolator based on one-way space-time coherency

Sajjad Taravati

Department of Electrical Engineering, Poly-Grames Research Center, Polytechnique Montréal, Montréal, QC, Canada

(Received 19 October 2017; published 29 December 2017)

This paper introduces a self-biased broadband magnet-free and linear isolator based on one-way space-time coherency. The incident wave and the space-time-modulated medium share the same temporal frequency and are hence temporally coherent. However, thanks to the unidirectionality of the space-time modulation, the space-time-modulated medium and the incident wave are spatially coherent only in the forward direction and not in the opposite direction. As a consequence, the energy of the medium strongly couples to the propagating wave in the forward direction, while it conflicts with the propagating wave in the opposite direction, yielding strong isolation. We first derive a closed-form solution for the wave scattering from a spatiotemporally coherent medium and then show that a perfectly coherent space-time-modulated medium provides a moderate isolation level which is also subject to one-way transmission gain. To overcome this issue, we next investigate the effect of space-coherency imperfection between the medium and the wave, while they are still perfectly temporally coherent. Leveraging the spatial-coherency imperfection, the medium exhibits a quasiarbitrary and strong nonreciprocal transmission. Finally, we present the experimental demonstration of the self-biased version of the proposed broadband isolator, exhibiting more than 122% fractional operation bandwidth.

DOI: [10.1103/PhysRevB.96.235150](https://doi.org/10.1103/PhysRevB.96.235150)**I. INTRODUCTION**

Creating nonreciprocal devices and isolators requires simultaneous breaking of both the time-reversal symmetry and the spatial inversion symmetry. This is conventionally achieved using magneto-optical materials possessing an asymmetric permittivity tensor [1–5], magnetically biased ferrites [6,7], and magnetically biased two-dimensional (2D) electron gas (2DEG) systems [8,9]. However, on-chip integration of magneto-optical materials is still difficult to achieve, particularly in silicon, which is compatible with complementary metal-oxide semiconductor technology. Magnetically biased isolators exhibit high power handling and high isolation, but they require bulky magnets and are incompatible with integrated circuit technology [10]. Two alternative approaches are transistor-based isolators [11–13] and nonlinear isolators [14–19], which eliminate the bulky magnet and are compatible with integrated circuit technology. However, the active transistor-based technology suffers from limited power handling and noise performance and its application to high frequencies and optics is impeded by frequency limitations of transistors [11,13]. Nonlinear isolators, on the other hand, may operate at optical frequencies, but they only provide isolation to high power signals, while low-level signals pass through them reciprocally [20].

To overcome the restrictions associated with the aforementioned approaches, one can instead break the Lorentz reciprocity using magnet-free linear structures undergoing space-time modulation [21,22]. Such dynamic structures result in linear isolators with responses that are independent of the power of the input signal. Space-time-modulated media were initially studied in the context of traveling wave parametric amplifiers, where a transmission line with distributed shunt capacitance is electronically modulated in synchronism with the incident wave but at twice its frequency [23–26]. This topic has recently regained a surge of scientific interest due to recently discovered exotic phenomenon in these media, such

as for instance interband photonic transitions and associated nonreciprocal frequency generation [21,27].

The space-time modulation technique is compatible with circuit technology and integrated optical networks and has been recently utilized for realization of microwave and optical isolators [21,22,28–32], circulators [33], nonreciprocal metasurfaces [34–36], and nonreciprocal integrated components [37–39]. The operation of these components are mainly based on the interband photonic transitions provided by a space-time-modulated structure [21]. In a spatiotemporally modulated waveguide, the required energy and momentum is provided by the space-time modulation for making a transition from one mode to another mode. However, no transition occurs in the opposite direction as the provided energy and momentum does not correspond to another mode of the waveguide in the opposite direction. However, such a technique suffers from requiring a transversally asymmetric profile for the space-time-modulated region. In addition, its application as an isolator requires a bandpass filter. Intraband transitions, a transition from one mode to itself, does not require any transverse asymmetry and hence easier to fabricate. However, it is plagued with infinite number of undesirable space-time harmonics [22].

This paper introduces a new technique for achieving linear isolation based on unidirectional coherency between the incident wave and the space-time-modulated medium. The space-time modulation and the incident wave share the same temporal frequency, and are hence temporally coherent regardless of direction of the incident wave. As a result, the nonreciprocal operation of the structure is dictated by the spatial coherency difference between the unidirectionally space-time-modulated medium and the incident wave. At certain space-time modulation phase shifts and modulation depths, corresponding to the space-time coherency conditions, the structure operates as an isolator. The proposed structure provides broad operation bandwidth and small size and, hence, exhibits superior efficiency compared to previously

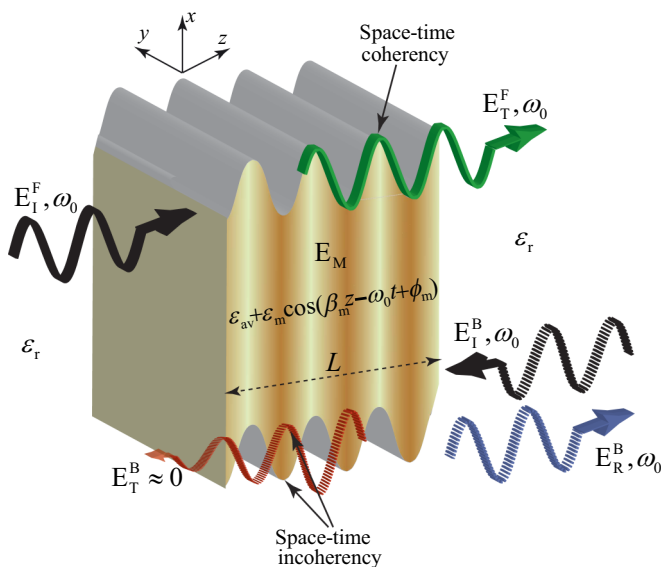


FIG. 1. Electromagnetic isolation based on nonreciprocal coherency of a plane wave with a periodically space-time-modulated medium. (Top) coherency between the space-time variations of the $+z$ propagating wave and the slab leads to full transmission of the wave. (Bottom) incoherency between the space-time variation of the $-z$ propagating wave and the slab yields reflection of the wave.

reported space-time isolators [21,22,30,32,34,35]. The input signal modulates the structure itself, and it thus operates as a self-biased isolator. Moreover, the proposed spatiotemporally coherent isolator is capable of providing transmission gain, as well as introducing nonreciprocal reflection gain, which may find various applications, particularly in radar, optics, nonreciprocal metasurfaces, and illusion cloaks. This paper exhibits the implementation of the microwave version of the proposed self-biased broadband spatiotemporally coherent isolator using varactors. Such a structure may be implemented in terahertz and optics using vanadium dioxide materials [40,41], which represents an interesting topic of research.

The paper is organized as follows. Section II presents the operation principle and Sec. III derives the closed form solution for nonreciprocal electromagnetic scattering from the isolator. Space-time coherency conditions are described in Sec. IV. Finally, Sec. V presents the experimental demonstration of both the externally biased and self-biased versions of the proposed isolator using a transmission line loaded with an array of space-time-modulated varactors.

II. OPERATION PRINCIPLE

Figure 1 shows a generic representation of the spatiotemporally coherent isolator. The isolator consists of a slab with thickness L and permittivity

$$\epsilon(z,t) = \epsilon_{av} + \epsilon_m \cos(\beta_m z - \omega_0 t + \phi_m), \quad (1)$$

sandwiched between two semi-infinite unmodulated media. In (1), ϵ_{av} denotes the average effective permittivity of the unmodulated slab, ϵ_m represents the modulation depth, ϕ_m is the modulation phase, and ω_0 and β_m are, respectively, the modulation temporal and spatial frequencies. Considering

the unidirectionality of the space-time modulation, with the modulation phase velocity of $v_m = \omega_0/\beta_m$, the structure is inherently nonreciprocal. The modulation phase velocity may be smaller or greater than the phase velocity of the background medium, $v_b = c/\sqrt{\epsilon_r}$, with ϵ_r and $c = 1/\sqrt{\mu_0\epsilon_0}$ being the relative permittivity and the speed of light in vacuum, respectively. We consider a y -polarized plane wave, represented by \mathbf{E}_I and temporal frequency ω_0 , as

$$\mathbf{E}_I(z,t) = \hat{\mathbf{y}} E_0 e^{-j(\beta_0 z - \omega_0 t)}, \quad (2)$$

impinging the periodically space-time-modulated slab in Fig. 1. In (2), E_0 represents the amplitude of the incident wave and β_0 is the spatial frequency of the wave in the unmodulated medium, i.e., $\beta_0 = \omega_0/v_b = \omega_0 c/\sqrt{\epsilon_r}$. We define the *velocity ratio* as the ratio between the modulation and background phase velocities [22], as

$$\gamma = \frac{v_m}{v_b} = \frac{\beta_0}{\beta_m} \sqrt{\frac{\epsilon_r}{\epsilon_{av}}}, \quad (3)$$

where

$$\beta_0 = \frac{\omega_0 \sqrt{\epsilon_r}}{c}, \quad (4)$$

is the spatial frequency of the wave outside the space-time-modulated medium, in the unmodulated regions with the permittivity ϵ_r , and

$$\beta_m = \frac{\omega_0 \sqrt{\epsilon_{av}}}{c\gamma}, \quad (5)$$

being the spatial modulation frequency in the modulated medium with the average permittivity ϵ_{av} . We call the problem with the incident wave propagating towards the $+z$ direction, shown in the top of Fig. 1, as the *forward problem*, denoted by the superscript “F,” while the problem with the incident wave propagating towards the $-z$ direction, shown in the bottom of Fig. 1, will be called the *backward problem*, denoted by the superscript “B.” It should be noted that the forward and backward problems both create forward and backward waves, inside and outside of the space-time-modulated slab. Here, the temporal frequency of the incident wave, ω_0 , and the one of the space-time-modulated medium are assumed to be equal, leading to perfect temporal coherency between the incident wave and the medium.

III. CLOSED-FORM SOLUTIONS FOR THE SCATTERED FIELDS

This section derives the scattered fields for the forward and backward problems shown in Fig. 1. We may consider a $+z$ propagating incident field, given in (2), for both forward and backward problems, whereas the forward problem assumes a $+z$ traveling modulation, [$\epsilon(z,t) = \epsilon_{av} + \epsilon_m \cos(\beta_m z - \omega_0 t + \phi_m)$], and the backward problem assumes a $-z$ traveling modulation as [$\epsilon(z,t) = \epsilon_{av} + \epsilon_m \cos(\beta_m z + \omega_0 t + \phi_m)$]. As shown in Sec. 1 of Ref. [42], considering the following transformation:

$$W = 2\gamma \sqrt{\frac{2\epsilon_m}{\epsilon_{av}}} e^{j(\beta_m z - \omega_0 t + \phi_m)/2}, \quad t' = t, \quad (6)$$

the electric field inside the spatiotemporally coherent medium reads

$$\mathbf{E}_M(W, t') = \hat{\mathbf{y}} A^{\text{F,B}}(t') I_\alpha(W) + \hat{\mathbf{y}} B^{\text{F,B}}(t') K_\alpha(W), \quad (7a)$$

where $I_\alpha(W)$ and $K_\alpha(W)$ are the modified Bessel functions of the first and second kinds which are the solutions to the modified Bessel differential equation in (S9a) in Ref. [42], with α defined as

$$\alpha = 2\gamma. \quad (7b)$$

The unknown field coefficients in (7a), $A^{\text{F,B}}$ and $B^{\text{F,B}}$, will be found by applying the spatial boundary conditions at $W = W_0 = W(z = 0, t)$ and $W = W_L = W(z = L, t)$, separately for forward and backward problems. We wish to calculate the fields scattered by the coherent space-time-modulated medium for forward and backward problems, namely the reflected fields, $\mathbf{E}_R^{\text{F,B}}$, and the transmitted fields, $\mathbf{E}_T^{\text{F,B}}$, as

$$\mathbf{E}_R^{\text{F,B}}(z, t') = \hat{\mathbf{y}} [A^{\text{F,B}} I_\alpha(W_0^{\text{F,B}}) - B^{\text{F,B}} K_\alpha(W_0^{\text{F,B}}) - E_0 e^{j\omega_0 t'}] \times e^{j\beta_0 z}, \quad (8a)$$

$$\mathbf{E}_T^{\text{F,B}}(z, t') = \hat{\mathbf{y}} [A^{\text{F,B}} I_\alpha(W_L^{\text{F,B}}) + B^{\text{F,B}} K_\alpha(W_L^{\text{F,B}})] e^{-j\beta_0(z-L)}, \quad (8b)$$

with

$$W_0^{\text{F}} = W_0^{\text{B}} = W(z = 0) = 2\gamma \sqrt{\frac{2\epsilon_m}{\epsilon_{\text{av}}}} e^{j(-\omega_0 t + \phi_m)/2} \quad (8c)$$

and

$$W_L^{\text{F,B}} = W(z = L) = 2\gamma \sqrt{\frac{2\epsilon_m}{\epsilon_{\text{av}}}} e^{j(\pm\beta_m L - \omega_0 t + \phi_m)/2}. \quad (8d)$$

The unknown field coefficients $A^{\text{F,B}}$ and $B^{\text{F,B}}$ are determined by satisfying the boundary conditions at $z = 0$ and $z = L$. These terms are derived in Sec. 2 of Ref. [42], as

$$A^{\text{F}} = B^{\text{F}} \frac{K_{\alpha+1}(W_L^{\text{F}})}{I_{\alpha+1}(W_L^{\text{F}})}, \quad (9a)$$

$$B^{\text{F}} = \frac{-2\alpha E_0 e^{j\omega_0 t'}}{W_0 [K_{\alpha-1}(W_0) - K_{\alpha+1}(W_L^{\text{F}}) I_{\alpha-1}(W_0) / I_{\alpha+1}(W_L^{\text{F}})]}, \quad (9b)$$

for the forward problem, and

$$A^{\text{B}} = B^{\text{B}} \frac{K_{\alpha-1}(W_L^{\text{B}})}{I_{\alpha-1}(W_L^{\text{B}})}, \quad (10a)$$

$$B^{\text{B}} = \frac{2\alpha E_0 e^{j\omega_0 t'}}{W_0 [K_{\alpha+1}(W_0) - K_{\alpha-1}(W_L^{\text{B}}) I_{\alpha+1}(W_0) / I_{\alpha-1}(W_L^{\text{B}})]}, \quad (10b)$$

for the backward problem. As expected from the unidirectionality of the space-time modulation in (1), $A^{\text{B}} \neq A^{\text{F}}$ and $B^{\text{B}} \neq B^{\text{F}}$. It may be simply verified that in the particular case where the spatial modulation frequency is switched off

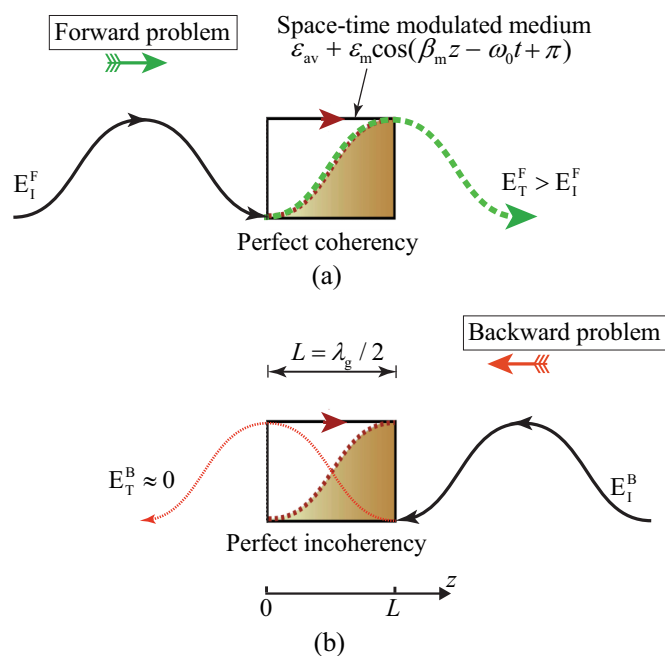


FIG. 2. One-way space-time coherency in the unidirectionally space-time-modulated medium in Fig. 1. The medium assumes length of $L = \lambda_g/2 = \pi v_b/\omega_0$ and modulation phase of $\phi_m = \pi$, $\epsilon_{\text{av}} = \epsilon_r$, and $\gamma = 1$. The temporal modulation frequency, ω_0 , of the medium is equal to the temporal frequency of the forward and backward incident waves $\mathbf{E}_i^{\text{B,F}}$, while the spatial modulation frequency, β_m , of the medium is equal to the spatial frequency of the forward incident wave, $\beta_m = \beta_0^{\text{F}}$, but opposite the spatial frequency of the backward incident wave, i.e., $\beta_m = -\beta_0^{\text{B}}$. (a) Forward problem: perfect coherency; and (b) backward problem: perfect incoherency.

($\beta_m = 0$), so that $W_L^{\text{B}} = W_L^{\text{F}}$, these inequalities transform to equalities, and therefore, represent the field coefficients of a reciprocal system.

It may be seen from (8b), with its coefficients in (9) to (10), that the medium is linear, where the output of the medium E_T linearly follows the input wave E_0 . Linearity represents one of the main advantages of spatiotemporally modulated isolators, in oppose to nonlinear isolators, where an appropriate isolation is provided for high power signals, while weak signals pass through them reciprocally [20].

IV. SPACE-TIME COHERENCY CONDITIONS

A. Perfect one-way space-time coherency ($\beta_m = \beta_0$)

Figure 2 illustrates the electromagnetic wave transmission through the unidirectionally coherent space-time-modulated medium. Consider the plane wave in (2) impinging in the space-time-modulated medium with the permittivity in (1), where the spatial modulation frequency, β_m , and the temporal modulation frequency, ω_0 , are respectively equal to the spatial frequency and temporal frequency of the incident electromagnetic wave \mathbf{E}_i , i.e., $\beta_m = \beta_0$. This means the incident wave and the modulation propagate at the same velocity, and, depending on the space-time modulation specifications, this may lead to constructive or destructive interference between the incident wave and the modulated medium. The medium

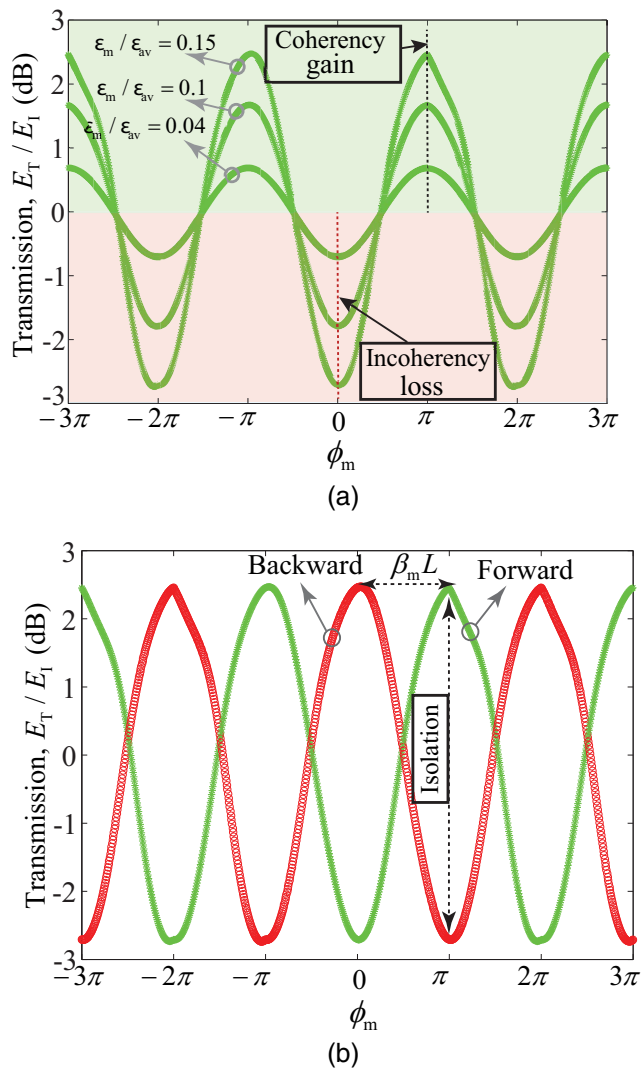


FIG. 3. Investigation of one-way space-time coherency in the medium shown in Fig. 2 with $L = \lambda_g/2 = \pi v_b/\omega_0$, $\epsilon_{av} = \epsilon_r = 7.06$, and $\omega_0 = 2\pi \times 2$ GHz. The spatial modulation frequency, β_m , and temporal modulation frequency, ω_0 , are respectively equal to the spatial frequency and temporal frequency of the excitation electromagnetic wave E_I ($\gamma = 1$). (a) Effect of the modulation phase, ϕ_m , on the forward transmission coherency for different modulation depths, i.e., $\epsilon_m/\epsilon_{av} = 0.04, 0.1$, and 0.15 . (b) Effect of the modulation phase, ϕ_m , on the forward and backward transmissions for $\epsilon_m/\epsilon_{av} = 0.15$.

assumes length of $L = \lambda_g/2 = \pi v_b/\omega_0$ and a modulation phase of $\phi_m = \pi$ and $\gamma = 1$. Figure 2 reveals that, such a unidirectional space-time-modulated medium provides perfect forward coherency and perfect backward incoherency. We aim to achieve an appropriate isolation between the forward and backward transmissions using proper modulation parameters, ϕ_m , ϵ_m , and $\beta_m L$.

To best understand the operation principle of the structure in Fig. 1, here we investigate the effect of the modulation phase ϕ_m on the forward and backward transmissions. Figure 3 plots the closed-form solution result for the transmitted field through the space-time-modulated medium in Fig. 2 versus the modulation phase ϕ_m . The length of the medium reads

$L = \lambda_g/2 = \pi v_b/\omega_0$, and the transmitted field is achieved for different modulation depths, $\epsilon_m/\epsilon_{av} = 0.04, 0.1$, and 0.15 . It may be seen from Fig. 3 that maximal forward space-time coherency gain is achieved for certain phase shifts where the medium and the electromagnetic wave are perfectly coherent, i.e., $\phi_m = (2n + 1)\pi$ with $n = 0, 1, \dots$. In contrast, maximal forward space-time coherency loss (reflection) is achieved for certain phase shifts where the medium and the electromagnetic wave are perfectly incoherent, i.e., $\phi_m = (2n)\pi$ with $n = 0, 1, \dots$. Interestingly, increasing the modulation depth ϵ_m/ϵ_{av} from 0.04 to 0.1 and 0.15 yields injection of more energy to the medium. As a result of the forward coherency, this energy will then couple to the forward propagating wave and yield higher transmission gain.

Figure 3(b) plots the closed-form solution results for both the forward and backward transmissions through the structure in Figs. 2 with the same parameters as in Fig. 3 and only for $\epsilon_m/\epsilon_{av} = 0.15$. Maximum isolation between the forward and backward propagating waves is achieved at the coherence phase shifts, whereas the forward wave is perfectly coherent with the medium, and the backward wave is perfectly incoherent with the medium. The length of the medium is considered as $L = \lambda_g/2$, which ensures maximal contrast between the forward and backward transmissions.

B. Design flexibility based on space-coherency imperfection ($\beta_m \neq \beta_0$)

The perfect spatiotemporally coherent medium in Fig. 2 (with $\beta_m \neq \beta_0$) provides moderate isolation between the forward and backward incident waves. However, the provided isolation level, shown in Fig. 3(b), may not be sufficient for most of the applications. Furthermore, the isolation is subject to the transmission gain, which may not be always desired. Therefore, this subsection investigates effect of the space-coherency imperfection, $\beta_m \neq \beta_0$ ($\gamma \neq 1$), on the operation of the temporally coherent medium in Fig. 1. We use the closed-form formulas in Sec. III to study the effect of different parameters on the nonreciprocal transmission. The space-coherency in the medium in Fig. 1 depends on its length L , the modulation phase ϕ_m , the velocity ratio γ , and the modulation depth ϵ_m .

Figure 4 plots the amplitude of the forward and backward transmitted waves versus the modulation depth for different velocity ratios, $\gamma = 1, 2, 6.66$, and 9 , computed using (8b) with $\phi_m = 1.318\pi$, $\epsilon_{av} = \epsilon_r = 7.06$, $\omega_0 = 2\pi \times 2$ GHz, and $L = 2\lambda_g$. To realize a coherent space-time-modulated isolator, we seek for the space-time modulation parameters corresponding to the unity forward transmission ($E_T^F/E_I \approx 0$ dB) and minimum backward transmission $E_T^B/E_I \ll E_T^F/E_I$. As we see in Fig. 4(c), forward transmission of $E_T^F/E_I = 0$ dB, corresponding to the isolation level of 24.5 dB, is achieved for $\gamma = 6.66$ and $\epsilon_m/\epsilon_r = 0.3$.

We next investigate the effect of the velocity ratio on the isolation between the forward and backward transmissions. Figure 5 plots the nonreciprocal transmission through the space-time-modulated medium in Fig. 1, computed using (8b), with the same parameters as in Fig. 4, except for varying γ and fixed modulation depth $\epsilon_m = 0.3\epsilon_{av}$. This figure shows that forward transmission of $E_T^F/E_I = 0$ dB with the isolation level of

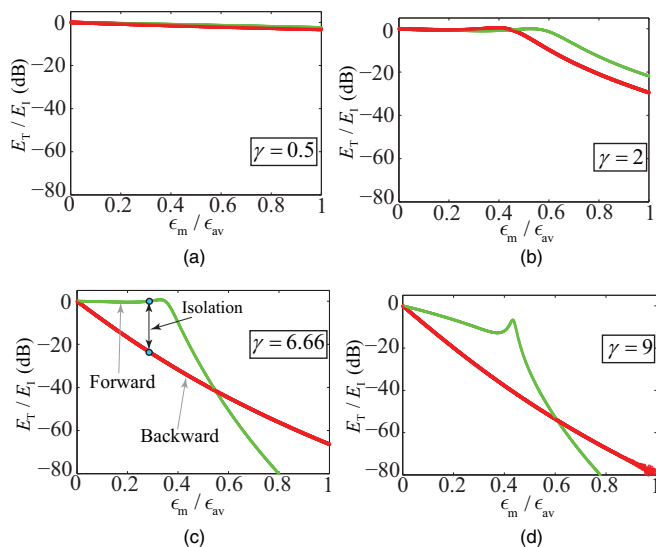


FIG. 4. Nonreciprocal transmission from the space-time-modulated isolator in Fig. 1 versus the modulation depth, computed using (8b) for $\phi_m = 1.318\pi$ and $L = 2\lambda_g$, $\epsilon_{av} = \epsilon_r = 7.06$, $\omega_0 = 2\pi \times 2$ GHz, and for different velocity ratios. (a) $\gamma = 0.5$. (b) $\gamma = 2$. (c) $\gamma = 6.66$. (d) $\gamma = 9$.

24.5 dB is achieved for $\gamma = 6.66$. A forward transmission peak is seen around $\gamma = 3.063$ which corresponds to perfect spatial coherency of forward wave, where $\beta_m L = \phi_m$. As Fig. 5 shows, a unidirectional periodically space-time-modulated medium exhibits reciprocal transmission as $\gamma \rightarrow \infty$ ($\beta_m \rightarrow 0$) and $\gamma \rightarrow 0$ ($\omega_{0,m} \rightarrow 0$) [22]. This observation is intuitively sensible. The nonreciprocity in a space-time-modulated medium is due to the unidirectionality of the space-time modulation, given by $\cos(\beta_m z - \omega_{0,m} t)$ in (1), whereas the space-time modulation becomes undirected as $\beta_m \rightarrow 0$ or $\omega_{0,m} \rightarrow 0$.

Figure 6 plots effect of the length L of the coherent space-time-modulated medium in Fig. 1 on forward and

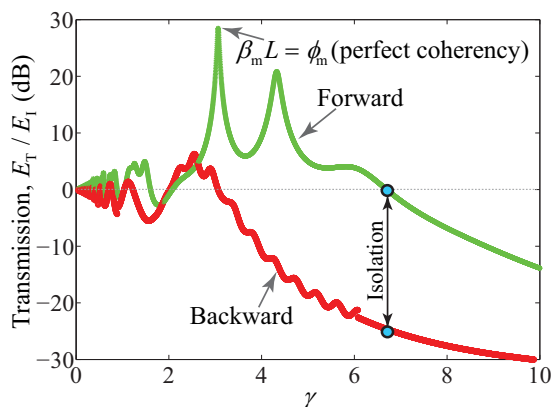


FIG. 5. Effect of the velocity ratio of the space-time-modulated isolator in Fig. 1 on forward and backward transmissions and isolation, computed using (8b), for the same parameters as in Fig. 4, except for varying γ and $\epsilon_m = 0.3\epsilon_{av}$. The peak of the forward transmission occurs at 3.063 which corresponds to perfect spatial coherency of forward wave, where $\beta_m L = \phi_m$.

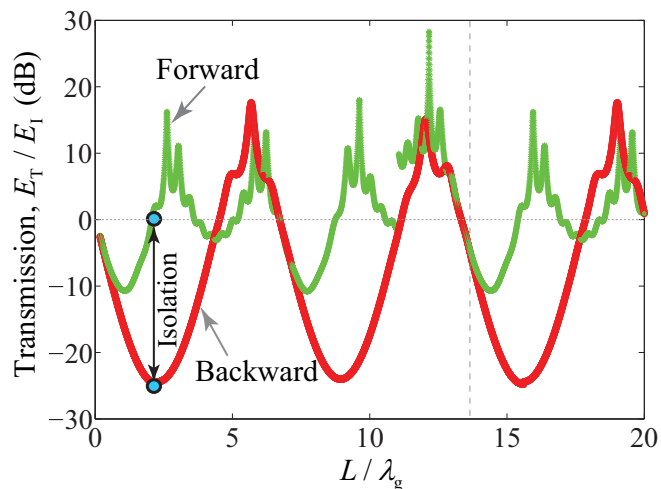


FIG. 6. Effect of the length L of the space-time-modulated medium in Fig. 1 on the forward and backward transmissions, computed using (8b), for the same parameters as in Fig. 5, except for varying L and fixed velocity ratio $\gamma = 6.66$.

backward transmissions, computed using (8b), considering the same parameters as in Figs. 5, except for varying L and fixed velocity ratio $\gamma = 6.66$. As expected, the forward and backward transmissions through the structure is a periodic function versus L , with a period of $L = 13.45\lambda_g$. Interestingly, depending on the length of the medium, it is capable of providing reciprocal transmission, $E_T^F/E_I = E_T^B/E_I$, e.g., for $L = 6.8\lambda_g$; nonreciprocal transmission with forward gain, $E_T^F/E_I > 0$ dB $> E_T^B/E_I$, e.g., for $L = 3\lambda_g$; and nonreciprocal transmission without forward gain, $E_T^F/E_I = 0$ dB $> E_T^B/E_I$, e.g., for $L = 2\lambda_g$. This represents an interesting functionality of the coherent space-time-modulated medium, as forward transmission gain may be desired in some applications.

Figure 7 plots effect of the modulation phase, ϕ_m , on the forward and backward transmissions through the medium in Fig. 1, computed using (8b), with the same parameters as in Fig. 6, except for varying ϕ_m and $L = 2\lambda_g$. As expected, the

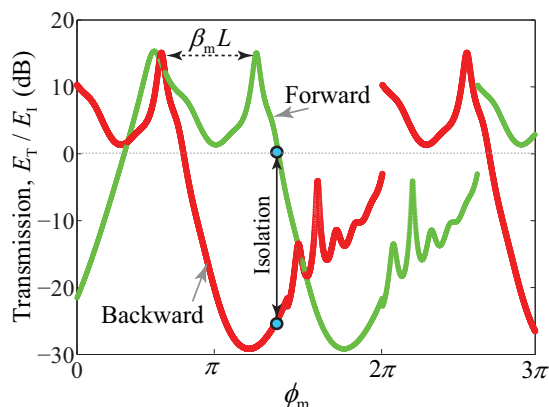


FIG. 7. Effect of the modulation phase, ϕ_m , of the space-time-modulated isolator in Fig. 1 on forward and backward transmissions, computed using (8b), for the same parameters as in Fig. 6, except for varying ϕ_m and $L = 2\lambda_g$.

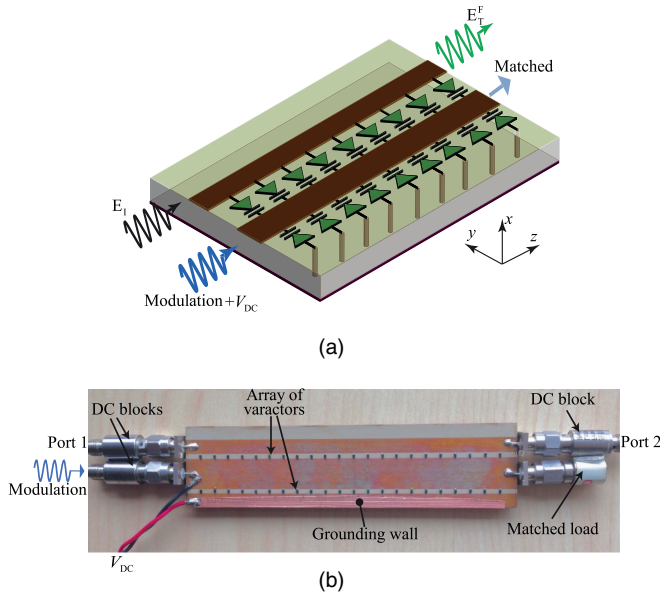


FIG. 8. Experimental demonstration of the externally biased spatiotemporally coherent isolator in Fig. 1 using microstrip technology. (a) Schematic of the system, with distributed varactors spatiotemporally modulated by a modulation wave launched at the same frequency as the input wave ω_0 . (b) Photograph of the fabricated isolator with the same coherent space-time modulation specifications as in Sec. IV B.

curves corresponding to forward and backward transmissions are a periodic function of ϕ_m , whereas the distance between the two forward and backward curves reads $\beta_m L$. Forward transmission of $E_T^F/E_I = 0$ dB with the isolation level of 24.5 dB is achieved for $\phi_m = 1.318\pi$.

V. EXPERIMENTAL DEMONSTRATION OF SELF-BIASED BROADBAND ISOLATOR

We next present the experimental implementation of the coherent space-time-modulated isolator in Fig. 1 with the space-time modulation specifications as in Sec. IV B. A possible implementation of the spatiotemporally coherent permittivity in (1) involves a transmission line loaded with an array of subwavelength-spaced antiparallel varactors distributed in parallel with the intrinsic capacitance of the transmission line. Figure 8(a) depicts the schematic of the system. An externally applied modulation wave with frequency ω_0 and wave vector β_m , propagating along $+z$ direction spatiotemporally modulates the varactors such as to provide the space-time varying capacitance $C(z, t) = C_{av} + C_{var} \cos(\beta_m z - \omega_0 t + \phi_m)$. As a result, the corresponding effective permittivity of the medium reads $\epsilon(z, t) = \epsilon_{av} + \epsilon_m \cos(\beta_m z - \omega_0 t + \phi_m)$, where the modulation depth, ϵ_m , depends on the range of variation of the varactors at a given modulation amplitude. In addition, a dc bias line sets the varactors in the reverse bias, capacitive, region and also provides the optimal average permittivity ϵ_{av} .

Figure 8(b) shows a photograph of the fabricated isolator. The modulation specifications are in accordance with Sec. IV B, i.e., $f_0 = \omega_0/2\pi = 2$ GHz, $\beta_m = 5.32\pi$, $L = 4.65$ in $= 2\lambda_g$, $\epsilon_m = 0.3\epsilon_{av}$, $\gamma = 6.66$, and $\phi_m = 1.318\pi$. The

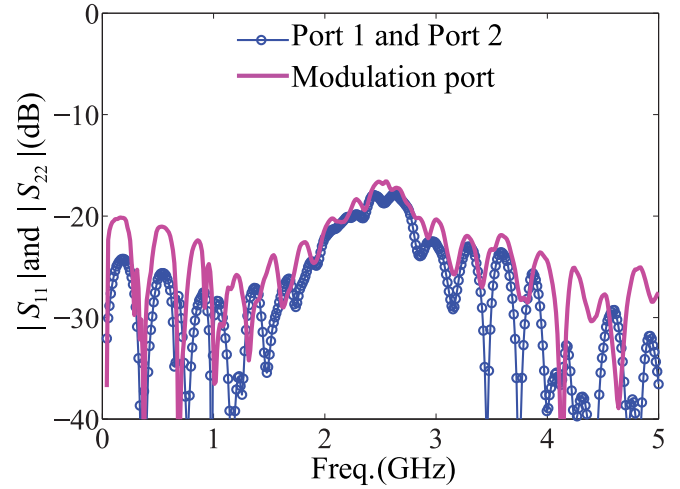


FIG. 9. Experimental matching of the signal and modulation ports of the isolator in Fig. 8.

modulation circuit is composed of 22 unit cells of antiparallel varactors, as shown in Fig. 8(a), with uniform spacing of $p = 5$ mm, which corresponds to $p/\lambda_g = p\beta_m/(2\pi) \approx 1/75.2$ and therefore satisfies medium homogeneity in accordance with (1). We employed SMV1247 varactors manufactured by Skyworks Solutions with the capacitance ratio $C_{max}/C_{min} = 10$. The specifications of the structure are RT6010 substrate with permittivity $\epsilon_{ef} = 7.06$, thickness $h = 100$ mil, and $\tan \delta = 0.0023$.

Figure 9 plots the experimental input matching of the two wave ports and the modulation port of the spatiotemporally coherent isolator in Figs. 8(a) and 8(b). These results are achieved by applying an optimal varactor dc bias of 3.8 V, which ensures the varactors safely operate in the linear reverse-biased regime, so that related nonlinear effects are negligible. It may be seen from Fig. 9 that input matching of more than 17 dB is achieved for the operation bandwidth from dc to 5 GHz, which ensures safe operation of the space-time modulation.

Figure 10(a) compares the analytical, simulation, and experimental results for forward and backward transmissions. It may be seen that forward transmission of $E_T^F/E_I^F = -0.56$ dB and backward transmission of $E_T^B/E_I^B = -26.3$ dB,

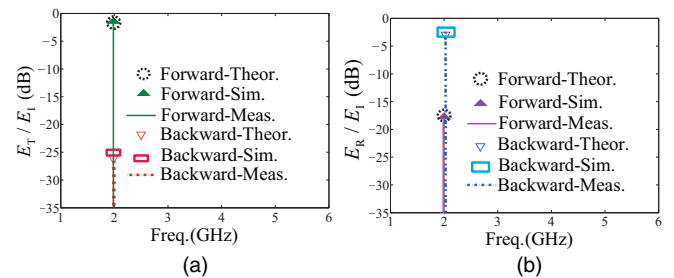


FIG. 10. Experimental results vs. simulation and theoretical results for the nonreciprocal transmission and reflection from the coherent space-time-modulated isolator in Fig. 8, with modulation specifications $\epsilon_m/\epsilon_{av} = 0.3$, $\phi_m = 1.318\pi$, $\gamma = 6.66$, and $L = 2\lambda_g$. (a) Nonreciprocal transmission. (b) Nonreciprocal reflection.

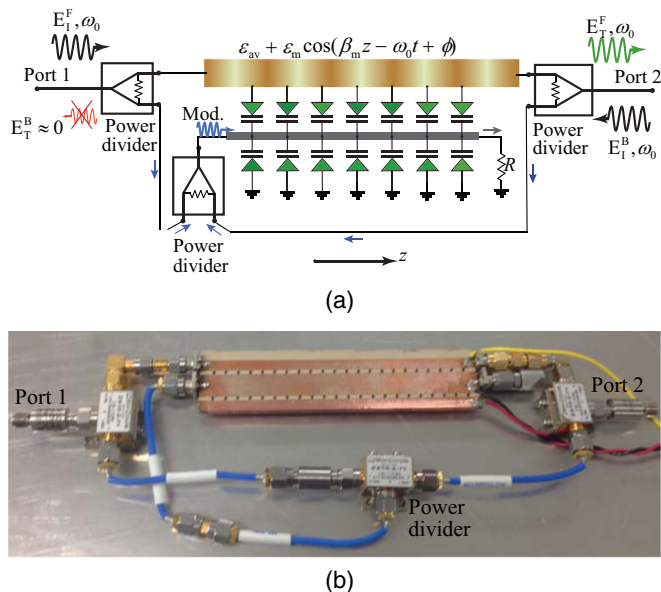


FIG. 11. Experimental realization of the self-biased coherent space-time-modulated isolator using the structure in Fig. 8 and three Wilkinson power dividers, with $\epsilon_m/\epsilon_{av} = 0.3$, $\phi_m = 1.318\pi$, $\gamma = 6.66$, and $L = 2\lambda_g$. (a) Schematic of the system, with distributed varactors spatiotemporally modulated by the modulation wave provided by the incident wave, emulating (1). (b) Photograph of the fabricated self-biased coherent space-time-modulated isolator.

corresponding to 25.74 isolation, is achieved. Figure 10(b) plots the corresponding nonreciprocal reflections for the forward and backward problems. Forward problem reflection of $E_R^F/E_I^F = -16.7$ dB and backward problem reflection of $E_R^B/E_I^B = -2.35$ dB, corresponding to the 25.74, is achieved. This reveals that the isolator passes the input wave in the forward problem, while reflects the input wave in the backward problem.

The isolator in Figs. 8(a) and 8(b) requires an external RF bias, with the same frequency as the input wave, to modulate the array of varactors. Therefore, we may take advantage of the perfect temporal coherency of the structure, employ the input signal as the source of the modulation wave, and realize a self-biased space-time-modulated isolator. Figure 11(a) illustrates the schematic of the proposed self-biased isolator. In this scheme, three Wilkinson power dividers are used to extract the modulation wave from the input wave. Figure 11(b) shows an image of the fabricated self-biased spatiotemporally coherent isolator.

We next investigate the operation bandwidth of the self-biased isolator in Fig. 11. Figure 12 plots the experimental and simulation results for the forward and backward transmissions through the spatiotemporally coherent isolator in Figs. 8(a) and 8(b), with the same parameters as in Fig. 11. As we see in Fig. 12, for the forward problem, the incident wave is almost fully transmitted with a transmission level of more than 6 dB from 0.8 to 3.3 GHz. For the backward problem, the backward incident wave is highly attenuated (reflected) with a attenuation level of more than 14 dB from 0.8 to 3.3 GHz. The experimental results correspond to more than 8 dB isolation across 122% fractional bandwidth.

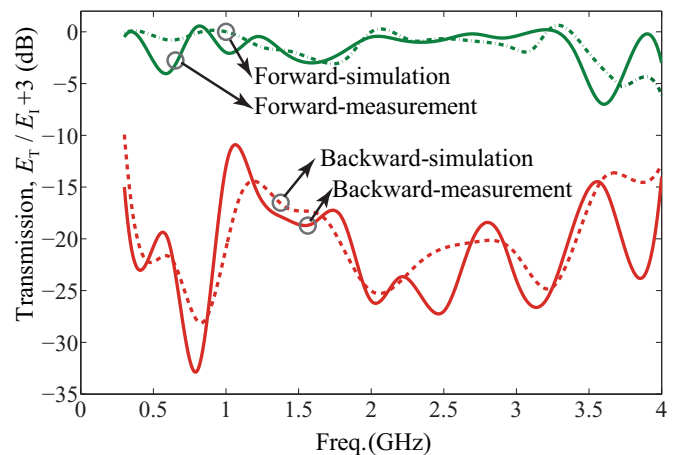


FIG. 12. Experimental vs. simulation results for the self-biased spatiotemporally coherent isolator in Fig. 11. Forward problem: The incident wave is almost fully transmitted with a transmission level of more than 6 dB from 0.8 to 3.3 GHz. Backward problem: The backward incident wave is highly attenuated (reflected) with an attenuation level of more than 14 dB from 0.8 to 3.3 GHz. The experimental results correspond to more than 8 dB isolation across 122% fractional operation bandwidth.

Higher isolation and transmission levels may be achieved by amplification of the extracted modulation wave, so that the structure experiences stronger modulation depth, ϵ_m/ϵ_{av} . The small discrepancy between the simulation and experimental results are attributed to the metallic and dielectric losses in the experiment and imperfect emulation of the space-time permittivity in (1).

VI. CONCLUSION

A self-biased broadband magnet-free linear isolator is proposed. The isolator operates based on the unidirectional space-time coherency, where the forward and backward incident waves both share the same temporal frequency with the space-time-modulated medium, and therefore, both are temporally-coherent with the medium. However, the space-time-modulated medium is spatially coherent only with the forward propagating wave, yielding transition of the energy from the medium to the forward transmitted wave. By contrast, the medium is spatially incoherent with the backward incident wave and thus conflicts with the backward incident wave, yielding strong attenuation of the backward traveling wave. A closed-form solution for the wave scattering from such a space-time coherent medium is derived. Taking advantage of imperfect space-coherency in the forward direction, the medium may introduce a quasiarbitrary nonreciprocal transmission. The experimental results of the proposed self-biased broadband isolator shows more than 122% fractional operation bandwidth. In addition, the structure is capable of providing nonreciprocal transmission gain as well as nonreciprocal reflection gain and may hence find complementary applications as in radar, nonreciprocal metasurfaces, and illusion cloaks.

- [1] R. L. Espinola, T. Izuhara, M.-C. Tsai, R. M. Osgood, and H. DÖtsch, Magneto-optical nonreciprocal phase shift in garnet/silicon-on-insulator waveguides, *Opt. Lett.* **29**, 941 (2004).
- [2] M. Levy, A nanomagnetic route to bias-magnet-free, on-chip faraday rotators, *J. Opt. Soc. Am. B* **22**, 254 (2005).
- [3] T. R. Zaman, X. Guo, and R. J. Ram, Faraday rotation in an InP waveguide, *Appl. Phys. Lett.* **90**, 023514 (2007).
- [4] Y. Shoji and T. Mizumoto, Ultra-wideband design of waveguide magneto-optical isolator operating in 1.31 μm and 1.55 μm band, *Opt. Express* **15**, 639 (2007).
- [5] Y. Shoji, T. Mizumoto, H. Yokoi, I. W. Hsieh, and R. M. Osgood, Magneto-optical isolator with silicon waveguides fabricated by direct bonding, *Appl. Phys. Lett.* **92**, 071117 (2008).
- [6] R. F. Soohoo, Microwave ferrite materials and devices, *IEEE Trans. Magn.* **4**, 118 (1968).
- [7] S. Capraro, T. Rouiller, M. L. Berre, J.-P. Chatelon, B. Bayard, D. Barbier, and J. J. Rousseau, Feasibility of an integrated self biased coplanar isolator with barium ferrite films, *IEEE Trans. Compon. Packag. Technol.* **30**, 411 (2007).
- [8] K. Suzuki and R. Hirota, Nonreciprocal millimeter-wave devices using a solid-state plasma at room temperature, *IEEE Trans. Electron Devices* **18**, 408 (1971).
- [9] G. N. Jawad, C. I. Duff, and R. Sloan, A millimeter-wave gyroelectric waveguide isolator, *IEEE Trans. Microw. Theory Techn.* **65**, 1249 (2017).
- [10] B. Lax and K. J. Button, *Microwave Ferrites and Ferrimagnetics* (McGraw-Hill, New York, 1962).
- [11] S. Tanaka, N. Shimomura, and K. Ohtake, Active circulators—the realization of circulators using transistors, *Proc. IEEE* **53**, 260 (1965).
- [12] Z. Wang, Z. Wang, J. Wang, B. Zhang, J. Huangfu, J. D. Joannopoulos, M. Soljaj, and L. Ran, Gyrotropic response in the absence of a bias field, *Proc. Natl. Acad. Sci. U.S.A.* **109**, 13194 (2012).
- [13] S. Taravati, B. A. Khan, S. Gupta, K. Achouri, and C. Caloz, Nonreciprocal nongyrotropic magnetless metasurface, *IEEE Trans. Antennas Propagat.* **65**, 3589 (2017).
- [14] M. Soljačić, C. Luo, J. D. Joannopoulos, and S. Fan, Nonlinear photonic crystal microdevices for optical integration, *Opt. Lett.* **28**, 637 (2003).
- [15] L. Fan, J. Wang, L. T. Varghese, H. Shen, B. Niu, Y. Xuan, A. M. Weiner, and M. Qi, An all-silicon passive optical diode, *Sci.* **335**, 447 (2012).
- [16] V. K. Valev, J. J. Baumberg, B. D. Clercq, N. Braz, X. Zheng, E. J. Osley, S. Vandendriessche, M. Hojiej, C. Blejean, C. G. Mertens, J. Biris, V. Volskiy, M. Ameloot, Y. Ekinci, G. A. E. Vandenbosch, P. A. Warburton, V. V. Moshchalkov, N. C. Panoiu, and T. Verbiest, Nonlinear superchiral meta-surfaces: Tuning chirality and disentangling non-reciprocity at the nanoscale, *Adv. Mate.* **26**, 4074 (2014).
- [17] L. Chang, X. Jiang, S. Hua, C. Yang, J. Wen, L. Jiang, G. Li, G. Wang, and M. Xiao, Paritytime symmetry and variable optical isolation in activepassive-coupled microresonators, *Nat. Photon.* **8**, 524 (2014).
- [18] A. M. Mahmoud, A. R. Davoyan, and N. Engheta, All-passive nonreciprocal metastructure, *Nat. Commun.* **6**, 8359 (2015).
- [19] Z.-M. Gu, J. Hu, B. Liang, X.-Y. Zou, and J.-C. Cheng, Broadband non-reciprocal transmission of sound with invariant frequency, *Sci. Rep.* **6**, 19824 (2016).
- [20] Y. Shi, Z. Yu, and S. Fan, Limitations of nonlinear optical isolators due to dynamic reciprocity, *Nat. Photon.* **9**, 388 (2015).
- [21] Z. Yu and S. Fan, Complete optical isolation created by indirect interband photonic transitions, *Nat. Photon.* **3**, 91 (2009).
- [22] S. Taravati, N. Chamanara, and C. Caloz, Nonreciprocal electromagnetic scattering from a periodically space-time-modulated slab and application to a quasisonic isolator, *Phys. Rev. B* **96**, 165144 (2017).
- [23] A. L. Cullen, A traveling-wave parametric amplifier, *Nature* **181**, 332 (1958).
- [24] W. H. Louisell and C. F. Quate, Parametric amplification of space charge waves, *Proc. IRE* **46**, 707 (1958).
- [25] P. K. Tien, Parametric amplification and frequency mixing in propagating circuits, *J. Appl. Phys.* **29**, 1347 (1958).
- [26] G. M. Roe and M. R. Boyd, Parametric energy conversion in distributed systems, *Proc. IRE* **47**, 1213 (1959).
- [27] J. N. Winn, S. Fan, J. D. Joannopoulos, and E. P. Ippen, Interband transitions in photonic crystals, *Phys. Rev. B* **59**, 1551 (1999).
- [28] X. Huang and S. Fan, Complete all-optical silica fiber isolator via stimulated Brillouin scattering, *J. Lightwave Technol.* **29**, 2267 (2011).
- [29] M. S. Kang, A. Butsch, and P. S. J. Russell, Reconfigurable light-driven opto-acoustic isolators in photonic crystal fibre, *Nat. Photon.* **5**, 549 (2011).
- [30] H. Lira, Z. Yu, S. Fan, and M. Lipson, Electrically driven nonreciprocity induced by interband photonic transition on a silicon chip, *Phys. Rev. Lett.* **109**, 033901 (2012).
- [31] C. G. Poulton, R. Pant, A. Byrnes, S. Fan, M. J. Steel, and B. J. Eggleton, Design for broadband on-chip isolator using stimulated Brillouin scattering in dispersion-engineered chalcogenide waveguides, *Opt. Express* **20**, 21 (2012).
- [32] N. Chamanara, S. Taravati, Z.-L. Deck-Léger, and C. Caloz, Optical isolation based on space-time engineered asymmetric photonic bandgaps, *Phys. Rev. B* **96**, 155409 (2017).
- [33] N. A. Estep, D. L. Sounas, J. Soric, and A. Alù, Magnetic-free non-reciprocity and isolation based on parametrically modulated coupled-resonator loops, *Nat. Photon.* **10**, 923 (2014).
- [34] Y. Hadad, D. L. Sounas, and A. Alù, Space-time gradient metasurfaces, *Phys. Rev. B* **92**, 100304 (2015).
- [35] Y. Shi and S. Fan, Dynamic non-reciprocal meta-surfaces with arbitrary phase reconfigurability based on photonic transition in meta-atoms, *Appl. Phys. Lett.* **108**, 021110 (2016).
- [36] Y. Shi, S. Han, and S. Fan, Optical circulation and isolation based on indirect photonic transitions of guided resonance modes, *ACS Photon.* **4**, 1639 (2017).
- [37] S. Taravati and C. Caloz, Space-time modulated nonreciprocal mixing, amplifying and scanning leaky-wave antenna system, in *IEEE AP-S International Symposium on Antennas and Propagation, Vancouver, Canada* (IEEE, Piscataway, NJ, 2015).
- [38] Y. Hadad, J. C. Soric, and A. Alù, Breaking temporal symmetries for emission and absorption, *Proc. Natl. Acad. Sci. U.S.A.* **113**, 3471 (2016).
- [39] S. Taravati and C. Caloz, Mixer-duplexer-antenna leaky-wave system based on periodic space-time modulation, *IEEE Trans. Antennas Propag.* **65**, 442 (2017).

- [40] M. Liu, H. Y. Hwang, H. Tao, A. C. Strikwerda, K. Fan, G. R. Keiser, A. J. Sternbach, K. G. West, S. Kittiwatanakul, J. Lu, S. A. Wolf, F. G. Omenetto, X. Zhang, K. A. Nelson, and R. D. Averitt, Terahertz-field-induced insulator-to-metal transition in vanadium dioxide metamaterial, *Nature* **487**, 345 (2012).
- [41] M. R. M. Hashemi, S.-H. Yang, T. Wang, N. Sepúlveda, and M. Jarrahi, Electronically-controlled beam-steering through vanadium dioxide metasurfaces, *Sci. Rep.* **6**, 35439 (2016).
- [42] See Supplemental Material at <http://link.aps.org/supplemental/10.1103/PhysRevB.96.235150> for detailed derivations.